

AN APPLICATION OF 3-D KINEMATICAL CONSERVATION LAWS: PROPAGATION OF A 3-D WAVEFRONT*

K. R. ARUN[†], M. LUKÁČOVÁ-MEDVIĐOVÁ[‡], PHOOLAN PRASAD[†], AND
S. V. RAGHURAMA RAO[§]

Abstract. Three-dimensional (3-D) kinematical conservation laws (KCL) are equations of evolution of a propagating surface Ω_t in three space dimensions. We start with a brief review of the 3-D KCL system and mention some of its properties relevant to this paper. The 3-D KCL, a system of six conservation laws, is an underdetermined system to which we add an energy transport equation for a small amplitude 3-D nonlinear wavefront propagating in a polytropic gas in a uniform state and at rest. We call the enlarged system of 3-D KCL with the energy transport equation *equations of weakly nonlinear ray theory (WNLRT)*. We highlight some interesting properties of the eigenstructure of the equations of WNLRT, but the main aim of this paper is to test the numerical efficacy of this system of seven conservation laws. We take several initial shapes for a nonlinear wavefront with a suitable amplitude distribution on it and let it evolve according to the 3-D WNLRT. The 3-D WNLRT is a weakly hyperbolic 7×7 system that is highly nonlinear. Here we use the staggered Lax–Friedrichs and Nessyahu–Tadmor central schemes and have obtained some very interesting shapes of the wavefronts. We find the 3-D KCL to be suitable for solving many complex problems for which there presently seems to be no other method capable of giving such physically realistic features.

Key words. kinematical conservation laws, ray theory, nonlinear waves, kinks, weakly hyperbolic system, finite difference scheme

AMS subject classifications. Primary, 35L60, 35L65, 35L67, 35L80; Secondary, 58J47, 65M06

DOI. 10.1137/080732742

1. Introduction. Propagation of a nonlinear wavefront or a shock front in three-dimensional (3-D) (x_1, x_2, x_3) -space \mathbb{R}^3 is a very complex physical phenomenon. Both fronts share a common property of possessing curves of discontinuities across which the normal direction to the fronts and the amplitude distribution on them suffer discontinuities. These are discontinuities of the first kind, i.e., the limiting values of the discontinuous functions, and their derivatives on a front as we approach a curve of discontinuity from either side are finite. Such a discontinuity was first analyzed by Whitham in 1957 [34] (see also [35]), who called it shock-shock, meaning shock on a shock front. However, the theory of kinematical conservation laws shows that a discontinuity of this type is geometric in nature and can arise on any propagating surface Ω_t , and hence it has been given the general name *kink*. In order to explain the existence of a kink and study its formation and propagation, we need the governing equations in the form of a system of physically realistic conservation laws. In this

*Received by the editors August 14, 2008; accepted for publication (in revised form) May 8, 2010; published electronically July 15, 2010. This work was supported by the Department of Science and Technology (DST), Government of India, and the German Academic Exchange Service (DAAD).

<http://www.siam.org/journals/siap/70-7/73274.html>

[†]Department of Mathematics, Indian Institute of Science, Bangalore, 560012 India (arunkr@math.iisc.ernet.in, prasad@math.iisc.ernet.in). The work of the first author was funded by the Council of Scientific & Industrial Research (CSIR) under grant-09/079(2084)/2006-EMR-1. The work of the third author was supported by the Department of Atomic Energy, Government of India, under the Raja Ramanna Fellowship Scheme. The Department of Mathematics at IISc is partially supported by UGC under SAP.

[‡]Institute of Numerical Simulation, Hamburg University of Technology, D-21071 Hamburg, Germany (lukacova@tu-harburg.de).

[§]Department of Aerospace Engineering, Indian Institute of Science, Bangalore, 560012 India (raghu@aero.iisc.ernet.in).

paper we derive such conservation laws for a surface Ω_t evolving in \mathbb{R}^3 in a specially defined ray coordinate system. Since they are derived purely on geometrical consideration, they have been called the kinematical conservation laws (KCL) [3, 27]. When a discontinuous solution of the KCL system in the ray coordinates has a shock satisfying Rankine–Hugoniot conditions, the image of the shock in \mathbf{x} -space \mathbb{R}^3 is a kink.

Before we start any discussion, we assume that all variables, both dependent and independent, used in this paper are nondimensional, with the exception of the first paragraph in section 3.

The KCL governing the evolution of a moving curve Ω_t in two space dimensions (x_1, x_2) were first derived by Morton, Prasad, and Ravindran [25] in 1992, and the kink (in this case, a point on Ω_t) phenomenon is well understood [27]. We call this system of KCL a two-dimensional (2-D) KCL. Prasad and his collaborators have used the 2-D KCL to solve many interesting problems and have obtained many new results [5, 6, 7, 8, 24, 29].

The KCL for a surface evolving in three space dimensions (called 3-D KCL), a system of six conservation laws, was first obtained by Giles, Prasad, and Ravindran [17]. Later on the analysis of 3-D KCL was completed by Arun and Prasad [3], which we discuss briefly in the next section.

The aim of this paper is to demonstrate the applicability of the theory of 3-D KCL showing successive positions and interesting shapes of a nonlinear wavefront obtained by numerical solution of the KCL system along with a closure relation representing the conservation of energy in a ray tube. We call KCL with this closure relation *equations of weakly nonlinear ray theory (WNLRT)*, which we shall elaborate upon in section 3. The rest of this paper is organized as follows: In section 4 we discuss some properties of WNLRT. In section 5 we present our numerical schemes, and in section 6 we give the results of numerical experiments.

2. 3-D KCL of Giles, Prasad, and Ravindran [17]. Consider a one-parameter family of surfaces Ω_t in (x_1, x_2, x_3) -space, where the subscript t is a parameter whose different values correspond to different positions of a moving surface. Let \mathbf{n} be the unit normal to Ω_t , and let $\boldsymbol{\chi}$ be a vector field called a ray vector field in \mathbf{x} -space. For simplicity, we assume $\boldsymbol{\chi}$ to be in the direction of \mathbf{n} , i.e.,

$$(2.1) \quad \boldsymbol{\chi} = m\mathbf{n},$$

where m is a scalar. We assume that evolution of Ω_t takes place by motion of its points moving with the ray velocity, i.e., according to

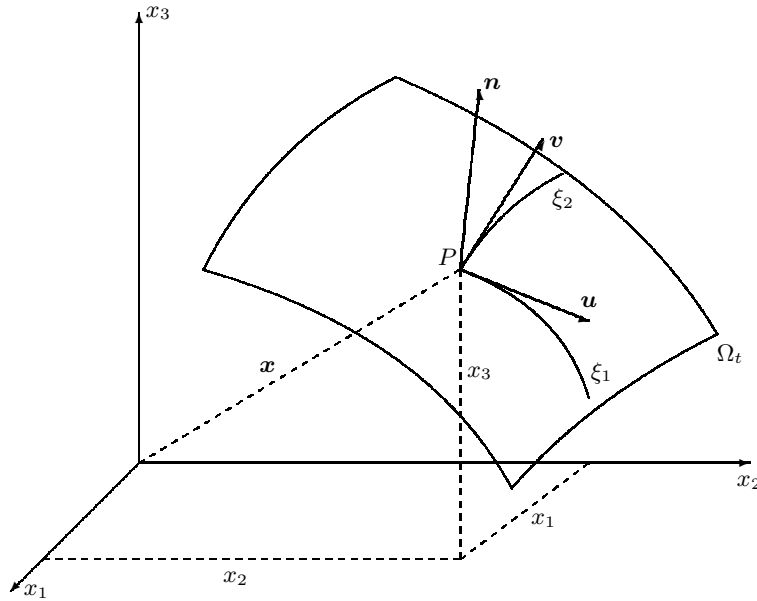
$$(2.2) \quad \frac{d\mathbf{x}}{dt} = m\mathbf{n}.$$

If Ω_t is given by $\Omega_t: \varphi(\mathbf{x}, t) = 0$, then φ satisfies the eikonal equation $\varphi_t + m|\nabla\varphi| = 0$. From the Hamilton's canonical equations (or the Charpit's equations) of this Hamilton–Jacobi equation we can derive [28]

$$(2.3) \quad \frac{d\mathbf{n}}{dt} = -(\nabla - \mathbf{n}\langle\mathbf{n}, \nabla\rangle)m.$$

Equations (2.2)–(2.3) form the set of ray equations. Given the initial position $\Omega_0: \mathbf{x} = \mathbf{x}_0(\xi_1, \xi_2)$, we can evaluate its normal $\mathbf{n} = \mathbf{n}_0(\xi_1, \xi_2)$ and then solve the ray equations (2.2)–(2.3) to get a parametric representation of Ω_t in the form

$$(2.4) \quad \Omega_t: \mathbf{x} = \mathbf{x}(\xi_1, \xi_2, t).$$

FIG. 2.1. A ray coordinate system on a surface Ω_t .

Thus, we have introduced a ray coordinate system (ξ_1, ξ_2, t) on Ω_t . Let \mathbf{u} and \mathbf{v} be, respectively, the unit tangent vectors of the curves $\xi_2 = \text{constant}$ and $\xi_1 = \text{constant}$ on Ω_t ; see Figure 2.1. The unit normal \mathbf{n} to Ω_t is then given by

$$(2.5) \quad \mathbf{n} = \frac{\mathbf{u} \times \mathbf{v}}{|\mathbf{u} \times \mathbf{v}|}.$$

Let an element of length along a curve ($\xi_2 = \text{constant}$, $t = \text{constant}$) be $g_1 d\xi_1$ and that along a curve ($\xi_1 = \text{constant}$, $t = \text{constant}$) be $g_2 d\xi_2$. The element of length along a ray ($\xi_1 = \text{constant}$, $\xi_2 = \text{constant}$) is $m dt$, since m is the velocity of the surface Ω_t . The displacement $d\mathbf{x}$ in \mathbf{x} -space due to increments $d\xi_1$, $d\xi_2$, and dt is given by

$$(2.6) \quad d\mathbf{x} = (g_1 \mathbf{u}) d\xi_1 + (g_2 \mathbf{v}) d\xi_2 + (m \mathbf{n}) dt.$$

This gives

$$(2.7) \quad J := \frac{\partial(x_1, x_2, x_3)}{\partial(\xi_1, \xi_2, t)} = g_1 g_2 m \sin \chi, \quad 0 < \chi < \pi,$$

where $\chi(\xi_1, \xi_2, t)$ is the angle between \mathbf{u} and \mathbf{v} , i.e.,

$$(2.8) \quad \cos \chi = \langle \mathbf{u}, \mathbf{v} \rangle.$$

As explained after (3.7), we shall choose $\sin \chi = |\mathbf{u} \times \mathbf{v}|$, which requires the restriction $0 < \chi < \pi$ on χ .

For a smooth moving surface Ω_t , we equate $\mathbf{x}_{\xi_1 t} = \mathbf{x}_{t \xi_1}$ and $\mathbf{x}_{\xi_2 t} = \mathbf{x}_{t \xi_2}$ and get the 3-D KCL of Giles, Prasad, and Ravindran [17],

$$(2.9) \quad (g_1 \mathbf{u})_t - (m \mathbf{n})_{\xi_1} = 0,$$

$$(2.10) \quad (g_2 \mathbf{v})_t - (m \mathbf{n})_{\xi_2} = 0.$$

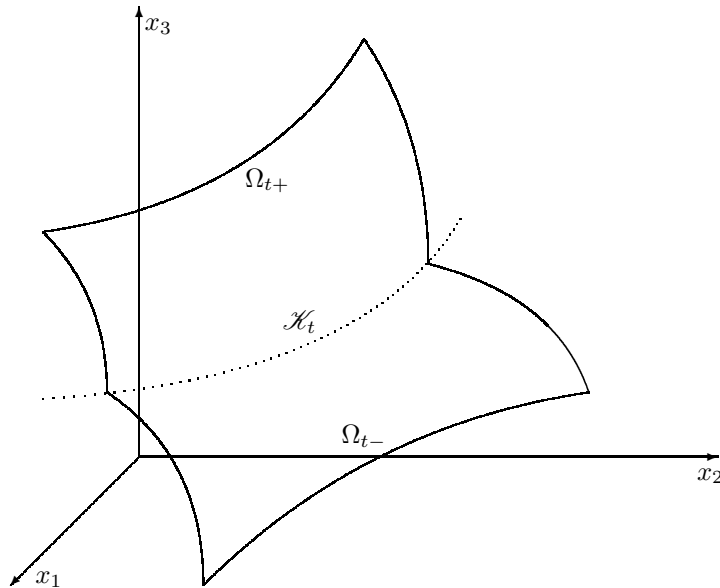


FIG. 2.2. Kink curve \mathcal{K}_t (shown with dotted line) on $\Omega_t = \Omega_{t+} \cup \Omega_{t-}$.

We also equate $\mathbf{x}_{\xi_1 \xi_2} = \mathbf{x}_{\xi_2 \xi_1}$ and derive three more scalar equations contained in

$$(2.11) \quad (g_2 \mathbf{v})_{\xi_1} - (g_1 \mathbf{u})_{\xi_2} = 0.$$

Equations (2.9)–(2.11) are necessary and sufficient conditions for the integrability of (2.6); see [13].

From (2.9)–(2.10) we can show that $(g_2 \mathbf{v})_{\xi_1} - (g_1 \mathbf{u})_{\xi_2}$ does not depend on t . Existence of coordinates ξ_1 and ξ_2 on Ω_0 guarantees that the condition (2.11) is satisfied at $t = 0$. Now (2.9)–(2.10) imply that (2.11) is satisfied for all t . Thus, the 3-D KCL is a system of six scalar evolution equations (2.9)–(2.10). However, since $|\mathbf{u}| = 1$, $|\mathbf{v}| = 1$, there are seven dependent variables in (2.9)–(2.10): two independent components of each of \mathbf{u} and \mathbf{v} , the front velocity m of Ω_t , and g_1 and g_2 . Thus, KCL is an underdetermined system and can be closed only with the help of additional relations or equations, which would follow from the nature of the surface Ω_t and the dynamics of the medium in which it propagates.

We derive a few results from (2.9)–(2.10) without considering the closure equation (or equations) for m . The system (2.9)–(2.10) consists of equations which are conservation laws, so its weak solution may contain shocks which are surfaces in (ξ_1, ξ_2, t) -space. Across these shock surfaces m, g_1, g_2 and vectors \mathbf{u}, \mathbf{v} , and \mathbf{n} will be discontinuous. The image of a shock surface into \mathbf{x} -space will be another surface¹—let us call it a kink surface—which will intersect Ω_t in a curve, say kink curve \mathcal{K}_t . Across this kink curve, or simply the kink, the normal direction \mathbf{n} of Ω_t will be discontinuous, as shown in Figure 2.2. As time t evolves, \mathcal{K}_t will generate the kink surface. A shock front (a phrase very commonly used in the literature) is a curve in the (ξ_1, ξ_2) -plane, and its motion as t changes generates the shock surface in (ξ_1, ξ_2, t) -space. In the derivation of (2.9)–(2.11) we assume that the mapping between (ξ_1, ξ_2, t) -space and (x_1, x_2, x_3) -space is one to one. This remains true locally even when a kink appears.

¹The mapping from (ξ_1, ξ_2, t) -space to \mathbf{x} -space is given by integration of (2.2).

However, if we have functions \mathbf{u} , \mathbf{v} , g_1 , g_2 , and m which satisfy (2.9)–(2.10), the mapping from (ξ_1, ξ_2, t) -space to (x_1, x_2, x_3) -space with the help of (2.2) may develop folds with kinks and cusps.

The distance $d\mathbf{x}$ between two points $P(\mathbf{x})$ and $Q'(\mathbf{x} + d\mathbf{x})$ on Ω_t and Ω_{t+dt} , respectively, satisfies the relation (2.6), where (ξ_1, ξ_2, t) and $(\xi_1 + d\xi_1, \xi_2 + d\xi_2, t + dt)$ are corresponding coordinates in (ξ_1, ξ_2, t) -space. If the points P and Q' are chosen to be points on the kink surface (see [27] for a 2-D analogue), then the conservation of $d\mathbf{x}$ implies that the expression for $(d\mathbf{x})_+$ on one side of the kink surface must be equal to the expression for $(d\mathbf{x})_-$ on the other side. Denoting quantities on the two sides of the kink by subscripts $+$ and $-$, we get

$$(2.12) \quad \begin{aligned} g_{1+} d\xi_1 \mathbf{u}_+ + g_{2+} d\xi_2 \mathbf{v}_+ + m_+ dt \mathbf{n}_+ \\ = g_{1-} d\xi_1 \mathbf{u}_- + g_{2-} d\xi_2 \mathbf{v}_- + m_- dt \mathbf{n}_-. \end{aligned}$$

We take the direction of the line element PQ' such that its projection onto the (ξ_1, ξ_2) -plane is in the direction of the normal to the shock curve in the (ξ_1, ξ_2) -plane; then the differentials are further restricted. Let the unit normal of this shock curve be (E_1, E_2) , and let K be its velocity of propagation in this plane; then the differentials in (2.12) satisfy $\frac{d\xi_1}{dt} = E_1 K$ and $\frac{d\xi_2}{dt} = E_2 K$, and (2.12) now becomes

$$(2.13) \quad \begin{aligned} (g_{1+} E_1 \mathbf{u}_+ + g_{2+} E_2 \mathbf{v}_+) K + m_+ \mathbf{n}_+ \\ = (g_{1-} E_1 \mathbf{u}_- + g_{2-} E_2 \mathbf{v}_-) K + m_- \mathbf{n}_-. \end{aligned}$$

Thus, (2.13) is a condition for the conservation of distance (in three independent directions in \mathbf{x} -space) across a kink surface when a point moves along the normal to the shock curve in the (ξ_1, ξ_2) -plane.

Using the usual method for the derivation of jump conditions across a shock, we deduce from the conservation laws (2.9)–(2.10) that

$$(2.14) \quad K[g_1 \mathbf{u}] + E_1[m\mathbf{n}] = 0, \quad K[g_2 \mathbf{v}] + E_2[m\mathbf{n}] = 0,$$

where a jump $[f]$ of a quantity f is defined by

$$(2.15) \quad [f] = f_+ - f_-.$$

Multiplying the first relation in (2.14) by E_1 and the second relation by E_2 , adding and using $E_1^2 + E_2^2 = 1$, we get

$$(2.16) \quad E_1 K[g_1 \mathbf{u}] + E_2 K[g_2 \mathbf{v}] + [m\mathbf{n}] = 0,$$

which is the same as (2.13). Thus we have proved the following theorem; see also [17].

THEOREM 2.1. *The six jump relations (2.14) imply conservation of distance in the x_1 , x_2 , and x_3 directions (and hence in any arbitrary direction in \mathbf{x} -space) in the sense that the expressions for a vector displacement $(d\mathbf{x})_{\mathcal{X}_t}$ of a point of the kink line \mathcal{X}_t in an infinitesimal time interval dt , when computed in terms of variables on the two sides of a kink surface, have the same value. This displacement of the point is assumed to take place on the kink surface, and that of its image in (ξ_1, ξ_2, t) -space takes place on the shock surface such that the corresponding displacement in the (ξ_1, ξ_2) -plane is in direction $\frac{d}{dt}(\xi_1, \xi_2) = (E_1, E_2)K$ so that the displacement remains on the shock front.*

This theorem ensures that the 3-D KCL are physically realistic. Consider a point P on a kink line \mathcal{X}_t on Ω_t and two straight lines T_- and T_+ orthogonal to the kink

line at P and lying in the tangent planes at P to Ω_{t-} and Ω_{t+} on the two sides of \mathcal{K}_t . Let N_- and N_+ be normals to the two tangent planes at P . Then the four lines T_+ , N_+ , N_- , and T_- , being orthogonal to the kink line at P , are coplanar. A kink phenomenon is basically 2-D. Locally, the two sides Ω_{t-} and Ω_{t+} of Ω_t can be regarded to be planes separated by a straight kink line. Hence the evolution of the kink phenomena can be viewed locally in a plane which intersects the planes Ω_{t-} , Ω_{t+} , and \mathcal{K}_t orthogonally, as shown in Figure 3.3.4 of [27].

We state an important result which has been found to be very useful in proving many properties of the KCL and in setting up the Cauchy data on Ω_0 . *Let $P_0(\mathbf{x}_0)$ be a given point on Ω_t at any time t . Then there exist two one-parameter families of smooth curves on Ω_t such that the unit vectors \mathbf{u}_0 and \mathbf{v}_0 along the members of the two families through the chosen point P_0 can have any two arbitrary directions, and the metrics g_{10} and g_{20} at this point can have any two positive values.*

3. Energy transport equation from a WNLRT for a polytropic gas and the complete set of equations. In this section we shall derive a closure relation in conservation form for the 3-D KCL so that we get a completely determined system of conservation laws. We take a simpler case of a nonlinear wavefront and not a shock front. We have explained the distinction between these two clearly in our previous publication [27, section 1.8]. Let the mass density, fluid velocity, gas pressure, and local sound velocity of a polytropic gas be denoted by ϱ , \mathbf{q} , p , and a . Assume that initially the gas is in a uniform state and at rest, i.e., $\varrho_0 = \text{constant}$, $\mathbf{q}_0 = 0$, and $p_0 = \text{constant}$. Consider a member Ω_t of a one-parameter family of curved nonlinear wavefronts in a small amplitude wave [27] moving with the characteristic velocity $\mathbf{q} + a\mathbf{n}$ running into the gas. A perturbation in the state of the gas on Ω_t under high frequency approximation can be expressed in terms of an amplitude w and is given by

$$(3.1) \quad \varrho - \varrho_0 = \left(\frac{\varrho_0}{a_0}\right)w, \quad \mathbf{q} = \mathbf{n}w, \quad p - p_0 = \varrho_0 a_0 w,$$

where a_0 is the sound velocity in the undisturbed medium $= \sqrt{\gamma p_0/\varrho_0}$ and w is a quantity of small order, say $\mathcal{O}(\epsilon)$. Let us recall what we stated in section 1: all dependent variables are dimensional in this (and only in this) paragraph. Note that w here has the dimension of velocity. The amplitude w is related to the nondimensional normal velocity m of Ω_t by

$$(3.2) \quad m = 1 + \frac{\gamma + 1}{2} \frac{w}{a_0}.$$

In the ray coordinate system, $\frac{\partial}{\partial t}$ represents the time rate of change as we move with the wavefront. Therefore the operator $\frac{d}{dt} = \frac{\partial}{\partial t} + m\langle \mathbf{n}, \nabla \rangle$ in space-time becomes simply the partial derivative $\frac{\partial}{\partial t}$ in the ray coordinate system (ξ_1, ξ_2, t) . Hence, the energy transport equation of the WNLRT [27] in nondimensional coordinates becomes

$$(3.3) \quad m_t = (m - 1)\Omega = -\frac{1}{2}(m - 1)\langle \nabla, \mathbf{n} \rangle,$$

where the italic symbol Ω is the mean curvature of the wavefront Ω_t . Consider a thin ray tube, i.e., a ray tube with a very small cross-sectional area as shown in Figure 3.1. Let δS be the cross-sectional area at a position t of the ray tube, and let δS_0 be that

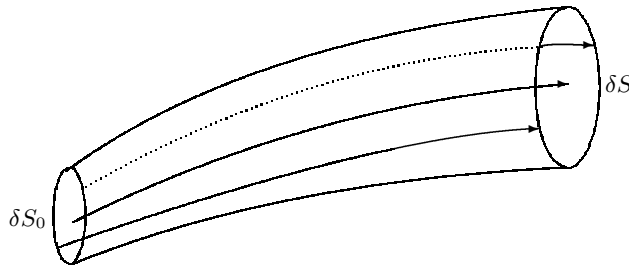


FIG. 3.1. Sketch of a ray tube.

at a reference section. The ray tube area \mathcal{A} is defined by [27, 35]

$$(3.4) \quad \mathcal{A} := \lim_{\delta S_0 \rightarrow 0} \frac{\delta S}{\delta S_0}.$$

The ray tube area of any ray system is related to the mean curvature Ω (we write here in nondimensional variables) by

$$(3.5) \quad \frac{1}{\mathcal{A}} \frac{\partial \mathcal{A}}{\partial l} = -2\Omega, \quad \frac{\partial}{\partial l} \text{ in ray coordinates,}$$

where l is the arc length along a ray. In nondimensional variables we have $dl = m dt$. From (3.3) and (3.5) we get

$$(3.6) \quad \frac{2m_t}{m-1} = -\frac{1}{m\mathcal{A}} \mathcal{A}_t.$$

This leads to a conservation law, which we accept to be the required one,

$$(3.7) \quad \left\{ (m-1)^2 e^{2(m-1)} \mathcal{A} \right\}_t = 0.$$

We note that, contrary to the result for the energy transport equation in the form $\left\{ (m-1)^2 \mathcal{A} \right\}_t = 0$ in a linear ray tube, we now have an addition factor $e^{2(m-1)}$ coming from nonlinear stretching of the rays.

Integration of (3.7) gives $(m-1)^2 e^{2(m-1)} \mathcal{A} = F(\xi_1, \xi_2)$, where F is an arbitrary function of ξ_1 and ξ_2 . The ray tube area \mathcal{A} is given by $\mathcal{A} = g_1 g_2 \sin \chi$, where χ is defined by (2.8). In order that \mathcal{A} be positive, we need to choose $0 < \chi < \pi$. The energy conservation equation (3.7) now becomes

$$(3.8) \quad \left\{ (m-1)^2 e^{2(m-1)} g_1 g_2 \sin \chi \right\}_t = 0.$$

Thus, the complete set of conservation laws for the weakly nonlinear ray theory (WNLRT) for a polytropic gas comprises the six equations in (2.9)–(2.10) and the equation (3.8). Equations (2.11) need to be satisfied at any fixed t , say at $t = 0$. Once we have a solution of this system in (ξ_1, ξ_2, t) -space, the results can be mapped into the \mathbf{x} -space by (2.2). This gives successive positions of the wavefront Ω_t .

4. Some properties of the system of equations of 3-D WNLRT and formulation of the ray coordinates for a particular surface. Our main aim in this paper is to get some interesting geometrical shapes of a propagating nonlinear wavefront in three dimensions by numerically solving the system of conservation laws

of 3-D WNLRT. However, in order to get a deeper understanding of WNLRT and to design an appropriate numerical scheme for this complex system, we need to know some of its important properties, which require a considerable amount of calculations and analysis. Hence, we simply quote these properties from [3]. We state the first result in the form of a theorem and refer to [3] for a proof.

THEOREM 4.1. *For a given smooth function m of \mathbf{x} and t , the ray equations (2.2) and (2.3) are equivalent to the KCL as long as their solutions are smooth.*

Note that (2.2) implies (2.3) with the help of an eikonal equation [28]. Theorem 4.1 is very interesting since ray equations follow from the theory of an eikonal equation (a partial differential equation for φ in \mathbb{R}^4 , where $\Omega: \varphi(\mathbf{x}, t) = 0$), whereas KCL is a purely geometric result.

The system of seven conservation laws—(2.9)–(2.10) and (3.8)—is quite complex. After considerable algebraic calculations, we can derive a system of seven differential equations which is given in the usual vector notation for the variable $V = (u_1, u_2, v_1, v_2, m, g_1, g_2)^T$ as

$$(4.1) \quad AV_t + B^{(1)}V_{\xi_1} + B^{(2)}V_{\xi_2} = 0,$$

where u_1, u_2 and v_1, v_2 are the first two components of the unit vectors \mathbf{u} and \mathbf{v} , respectively. The expressions for the matrices A , $B^{(1)}$, and $B^{(2)}$ are given in [3].

We can use also the above differential form of the KCL to deduce the ray equations. However, the most important use of (4.1) would be the derivation of eigenvalues and eigenvectors of the equations of WNLRT, which we state in the form of another theorem; see [3] for the proof.

THEOREM 4.2. *The system (4.1) has seven eigenvalues $\lambda_1, \lambda_2 (= -\lambda_1), \lambda_3 = \lambda_4 = \dots = \lambda_7 = 0$, where λ_1 and λ_2 are real for $m > 1$ and purely imaginary for $m < 1$. Further, the dimension of the eigenspace corresponding to the multiple eigenvalue 0 is 4.*

Since it has not been possible so far to factorize the characteristic equation for the eigenvalue λ of the system (4.1), namely, $\det(-\lambda A + e_1 B^{(1)} + e_2 B^{(2)}) = 0$, this result has been derived indirectly in [3]. First, due to the result mentioned at the end of section 2, we can first choose a fixed point P_0 on Ω_t in (x_1, x_2, x_3) -space. At this point, we take the $\xi_2 = \text{constant}$ and $\xi_1 = \text{constant}$ curves to be orthogonal, so that the unit tangent vectors $(\mathbf{u}, \mathbf{v})_{P_0} = (\mathbf{u}', \mathbf{v}')$ are orthogonal. The corresponding characteristic matrix can now be factorized and we can get the eigenvalues. Two eigenvalues turn out to be nonzero and distinct, and there is a zero eigenvalue with multiplicity five, but the dimension of the eigenspace corresponding to this multiple eigenvalue is only four. Now we can make a linear transformation from the orthogonal vectors $(\mathbf{u}', \mathbf{v}')$ to the general nonorthogonal vectors $(\mathbf{u}, \mathbf{v})_{P_0}$ in the tangent plane to Ω_t at P_0 and get the eigenvalues for an arbitrary coordinate system at this point. This procedure leads to the result stated in the above theorem; see [3] for more details.

The use of the transformation procedure mentioned in the above theorem leads to another deep result highlighting the relation between the eigenvalues appearing in a special formulation of a part of the ray equations, namely, (2.3) and the KCL [3]. We stop this discussion here as it takes us away from the main aim of this paper.

There is an extensive discussion of the above results in [3], which puts the theory of 3-D KCL on a strong mathematical foundation. In this paper we use 3-D KCL to discuss evolution of a weakly nonlinear wavefront Ω_t in three space dimensions and formation and propagation of curves of singularities on Ω_t . However, there is now a special challenge since Theorem 4.2 shows that the eigenspace of the eigenvalue 0

is not complete so that WNLRT equations are weakly hyperbolic. Theory of weakly hyperbolic systems is an active area of research, but it is very much incomplete; see [9, 11, 12, 14, 15, 18, 30, 32, 33] and the references therein; see also [10, 23] for numerical approximations of certain weakly hyperbolic systems. Appearance of δ -waves and δ -shocks in the solution of such systems may make the numerical approximation of weakly hyperbolic systems very complex; see [15]. The main aim of this paper is to show that in spite of possible difficulties which may arise due to the system being weakly hyperbolic, we have been able to develop numerical codes showing the efficacy of the 3-D WNLRT equations in conservation form.

Now we move on to the formulation of the ray coordinates on a given surface and show how to set up an initial value problem for the equations of WNLRT. Let the initial position of a weakly nonlinear wavefront Ω_t be given as

$$(4.2) \quad \Omega_0: x_3 = f(x_1, x_2).$$

On Ω_0 we choose $\xi_1 = x_1$, $\xi_2 = x_2$, then

$$(4.3) \quad \Omega_0: x_{10} = \xi_1, \quad x_{20} = \xi_2, \quad x_{30} = f(\xi_1, \xi_2)$$

and

$$(4.4) \quad \begin{aligned} g_{10} &= \sqrt{1 + f_{\xi_1}^2}, & g_{20} &= \sqrt{1 + f_{\xi_2}^2}, \\ \mathbf{u}_0 &= \frac{(1, 0, f_{\xi_1})}{\sqrt{1 + f_{\xi_1}^2}}, & \mathbf{v}_0 &= \frac{(0, 1, f_{\xi_2})}{\sqrt{1 + f_{\xi_2}^2}}. \end{aligned}$$

We can easily check that (2.11) is satisfied on Ω_0 . The unit normal \mathbf{n}_0 of Ω_0 is

$$(4.5) \quad \mathbf{n}_0 = -\frac{(f_{\xi_1}, f_{\xi_2}, -1)}{\sqrt{1 + f_{\xi_1}^2 + f_{\xi_2}^2}},$$

in which the sign is chosen such that $(\mathbf{u}, \mathbf{v}, \mathbf{n})$ form a right-handed system. Let the distribution of the front velocity be given by

$$(4.6) \quad m = m_0(\xi_1, \xi_2).$$

We have now completed formulation of the initial data for the KCL (2.9)–(2.10) and the energy transport equation (3.8).

The problem is to find a solution of the system (2.9)–(2.10) and (3.8) satisfying the initial data given by (4.4) and (4.6). Having solved these equations, we can get Ω_t by solving the first part of the ray equations, namely, (2.2) at least numerically for a number of values of ξ_1 and ξ_2 . In the next section we present an approximation of (2.9)–(2.10) and (3.8) using both the first order staggered Lax–Friedrichs scheme and the second order Nessyahu–Tadmor scheme.

5. Numerical approximation. Since we have an incomplete set of eigenvectors for the system (2.9)–(2.10), (3.8), the initial value problem is not well-posed in the strong hyperbolic sense and is likely to be more sensitive than regular hyperbolic systems from a computational point of view. Numerical as well as theoretical analysis indicates that the solution does not belong to BV spaces and is only measure valued. Despite theoretical difficulties, the aim of this section is to present a numerical solution

of the KCL (2.9)–(2.10) and (3.8) with initial data (4.4) and (4.6) using simple but robust central schemes. For a weakly hyperbolic system the central schemes are much more easily applicable than any characteristic-based scheme. Moreover, the simplicity of central finite volume schemes makes it convenient to employ them for the numerical solution of the complex system of conservation laws of WNLRT.

We will work with the first order staggered Lax–Friedrichs scheme [22] and the second order Nessyahu–Tadmor scheme [26]. Note that the KCL (2.9)–(2.10) and the energy transport equation (3.8) of WNLRT can be written as a system of conservation laws,

$$(5.1) \quad W_t + F_1(W)_{\xi_1} + F_2(W)_{\xi_2} = 0,$$

with the conserved variable W and the fluxes $F_i(W)$ given by

$$(5.2) \quad \begin{aligned} W &= \left(g_1 u_1, g_1 u_2, g_1 u_3, g_2 v_1, g_2 v_2, g_2 v_3, (m-1)^2 e^{2(m-1)} g_1 g_2 \sin \chi \right)^T, \\ F_1(W) &= (m n_1, m n_2, m n_3, 0, 0, 0, 0)^T, \\ F_2(W) &= (0, 0, 0, m n_1, m n_2, m n_3, 0)^T. \end{aligned}$$

Given the initial values of g_1 , g_2 , \mathbf{u} , \mathbf{v} , and m , the initial value of the conserved variable W is given by the first relation in (5.2). We numerically solve the system (5.1) to get the updated value of W . Since $|\mathbf{u}| = |\mathbf{v}| = 1$, from the first six components of W the values of g_1 , g_2 , \mathbf{u} , and \mathbf{v} can be computed very easily. The unit normal \mathbf{n} is then given by (2.5). To get the updated value of the normal velocity m we proceed as follows. Note that, say,

$$(5.3) \quad (m-1)^2 e^{2(m-1)} = \frac{W_7}{g_1 g_2 \sin \chi} \equiv k.$$

We now solve the nonlinear equation

$$(5.4) \quad \eta(m) \equiv (m-1)^2 e^{2(m-1)} - k = 0$$

for m using the Newton–Raphson method. The monotonicity of the function η in $(1, \infty)$ ensures the uniqueness of the solution of (5.4). Having obtained the values of m and \mathbf{n} , we numerically integrate the first part of the ray equations (2.2) to obtain the values of (x_1, x_2, x_3) , and this gives the successive position of the nonlinear wavefront Ω_t .

In what follows, we briefly review the staggered Lax–Friedrichs (LxF) scheme and the Nessyahu–Tadmor (NxT) scheme for the system of conservation laws (5.1) and refer to [2, 20, 21, 22, 26] for more details. Let us introduce a rectangular grid which for simplicity is assumed to be uniform with mesh size $h = \Delta \xi_1 = \Delta \xi_2$ in both directions. We will denote by $C_{i,j}$ the cell centered around the point (ξ_{1i}, ξ_{2j}) , i.e., $C_{i,j} = [\xi_{1i} - h/2, \xi_{1i} + h/2] \times [\xi_{2j} - h/2, \xi_{2j} + h/2]$. Let Δt be the time step and denote by $W_{i,j}^n$ the point value of W at the (i, j) th mesh point at time $t^n = n \Delta t$. Finally let $\bar{W}_{i,j}^n$ be the cell average of W taken over $C_{i,j}$, i.e.,

$$(5.5) \quad \bar{W}_{i,j}^n = \frac{1}{h^2} \int_{C_{i,j}} W(\xi_1, \xi_2, t^n) d\xi_1 d\xi_2.$$

Given the cell averages $\bar{W}_{i,j}^n$ at time level t^n , like the Godunov scheme, central schemes provide the cell averages at time level t^{n+1} in the following way. First a piecewise

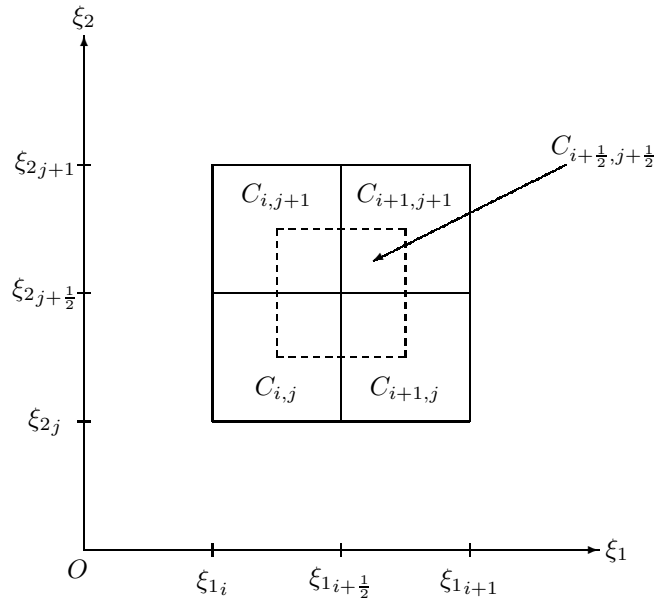


FIG. 5.1. A geometrical representation of the computational stencil: the original grid is depicted by solid lines and a staggered grid is denoted by dashed lines.

polynomial reconstruction is done, resulting in

$$(5.6) \quad W^n(\xi_1, \xi_2) = \sum_{i,j} P_{i,j}(\xi_1, \xi_2) \mathbf{1}_{i,j}(\xi_1, \xi_2),$$

where $P_{i,j}$ is some vector-valued polynomial and $\mathbf{1}_{i,j}$ is the characteristic function of the cell $C_{i,j}$.

In order to proceed, the reconstruction $W^n(\xi_1, \xi_2)$ is evolved according to (5.1) for a time step Δt . In central schemes, $W^n(\xi_1, \xi_2)$ is evolved on a staggered grid $C_{i+1/2,j+1/2} \times [t^n, t^{n+1}]$; see Figure 5.1. We will assume that the solution remains smooth along the edges of the staggered control volume, provided Δt satisfies the CFL condition

$$(5.7) \quad \frac{\Delta t}{h} \max(\rho_1, \rho_2) < \frac{1}{2},$$

where ρ_1 and ρ_2 are, respectively, the maximal propagation speeds in the ξ_1 - and ξ_2 -directions given by [4]

$$(5.8) \quad \rho_1 = \left(\frac{m-1}{2g_1^2 \sin^2 \chi} \right)^{\frac{1}{2}}, \quad \rho_2 = \left(\frac{m-1}{2g_2^2 \sin^2 \chi} \right)^{\frac{1}{2}}.$$

An exact integration of (5.1) with data $W^n(\xi_1, \xi_2)$ over the control volume $C_{i+1/2,j+1/2}$

$\times [t^n, t^{n+1}]$ yields the staggered update

$$(5.9) \quad \begin{aligned} \bar{W}_{i+\frac{1}{2},j+\frac{1}{2}}^{n+1} &= \frac{1}{h^2} \int_{C_{i,j}} W(\xi_1, \xi_2, t^n) d\xi_1 d\xi_2 \\ &\quad - \frac{1}{h^2} \int_{t^n}^{t^{n+1}} \left\{ \int_{\xi_{2j}}^{\xi_{2j+1}} [F_1(W(\xi_{1i+1}, \xi_2, \tau)) - F_1(W(\xi_{1i}, \xi_2, \tau))] d\xi_2 \right\} d\tau \\ &\quad - \frac{1}{h^2} \int_{t^n}^{t^{n+1}} \left\{ \int_{\xi_{1i}}^{\xi_{1i+1}} [F_2(W(\xi_1, \xi_{2j+1}, \tau)) - F_2(W(\xi_1, \xi_{2j}, \tau))] d\xi_1 \right\} d\tau. \end{aligned}$$

5.1. Lax–Friedrichs scheme. In the LxF scheme we use a piecewise constant data $\bar{W}_{i,j}^n$ over the cells $C_{i,j}$, i.e.,

$$(5.10) \quad W^n(\xi_1, \xi_2) = \sum_{i,j} \bar{W}_{i,j}^n \mathbf{1}_{i,j}(\xi_1, \xi_2).$$

Note that the first integral in (5.9) is the cell average of the function $W^n(\xi_1, \xi_2)$ over the staggered grid $C_{i+1/2,j+1/2}$. Given the reconstruction (5.10), this term can be computed exactly. The time integrals in (5.9) are approximated by the left rectangle rule and the space integrals by the trapezium rule, giving us the staggered LxF scheme

$$(5.11) \quad \begin{aligned} \bar{W}_{i+\frac{1}{2},j+\frac{1}{2}}^{n+1} &= \frac{1}{4} (\bar{W}_{i,j}^n + \bar{W}_{i+1,j}^n + \bar{W}_{i,j+1}^n + \bar{W}_{i+1,j+1}^n) \\ &\quad - \frac{\lambda_1}{2} (F_1(W_{i+1,j}^n) - F_1(W_{i,j}^n) + F_1(W_{i+1,j+1}^n) - F_1(W_{i,j+1}^n)) \\ &\quad - \frac{\lambda_2}{2} (F_2(W_{i,j+1}^n) - F_2(W_{i,j}^n) + F_2(W_{i+1,j+1}^n) - F_2(W_{i+1,j}^n)), \end{aligned}$$

where $\lambda_i = \Delta t / \Delta \xi_i$, $i = 1, 2$, are the mesh ratios.

5.2. Nessyahu–Tadmor scheme. The NxT scheme [2, 20, 21, 26] is a second order TVD extension of the LxF scheme. First, a piecewise linear interpolant is reconstructed from the given cell averages at time t^n ,

$$(5.12) \quad W(\xi_1, \xi_2, t^n) = \sum_{i,j} \left(\bar{W}_{i,j}^n + W'_{i,j} \left(\frac{\xi_1 - \xi_{1i}}{h} \right) + W^\wedge_{i,j} \left(\frac{\xi_2 - \xi_{2j}}{h} \right) \right) \mathbf{1}_{i,j}(\xi_1, \xi_2),$$

where $W'_{i,j}$ and $W^\wedge_{i,j}$ are, respectively, the discrete slopes in the ξ_1 - and ξ_2 -directions. A possible computation of these slopes which results in an overall nonoscillatory scheme is given by a family of discrete derivatives parametrized by $1 \leq \theta \leq 2$, for example,

$$(5.13) \quad \begin{aligned} W'_{i,j} &= MM \left\{ \theta (\bar{W}_{i+1,j}^n - \bar{W}_{i,j}^n), \frac{1}{2} (\bar{W}_{i+1,j}^n - \bar{W}_{i-1,j}^n), \theta (\bar{W}_{i,j}^n - \bar{W}_{i-1,j}^n) \right\}, \\ W^\wedge_{i,j} &= MM \left\{ \theta (\bar{W}_{i,j+1}^n - \bar{W}_{i,j}^n), \frac{1}{2} (\bar{W}_{i,j+1}^n - \bar{W}_{i,j-1}^n), \theta (\bar{W}_{i,j}^n - \bar{W}_{i,j-1}^n) \right\}. \end{aligned}$$

Here the nonlinear minmod function is defined by

$$(5.14) \quad MM \{v_1, v_2, \dots\} = \begin{cases} \min_p \{v_p\} & \text{if } v_p > 0 \ \forall p, \\ \max_p \{v_p\} & \text{if } v_p < 0 \ \forall p, \\ 0 & \text{otherwise.} \end{cases}$$

Another possibility to limit the numerical derivatives is to use a smooth CWENO (central weighted essentially nonoscillatory) limiter [19],

$$(5.15) \quad \begin{aligned} W'_{i,j} &= \text{CWENO} \{ (\bar{W}_{i+1,j}^n - \bar{W}_{i,j}^n), (\bar{W}_{i,j}^n - \bar{W}_{i-1,j}^n) \}, \\ W^\wedge_{i,j} &= \text{CWENO} \{ (\bar{W}_{i,j+1}^n - \bar{W}_{i,j}^n), (\bar{W}_{i,j}^n - \bar{W}_{i,j-1}^n) \}, \end{aligned}$$

where the CWENO function is defined by

$$(5.16) \quad \text{CWENO}(a, b) = \frac{\vartheta(a) \cdot a + \vartheta(b) \cdot b}{\vartheta(a) + \vartheta(b)}, \quad \vartheta(a) = (\epsilon + a^2)^{-2}, \quad \epsilon = 10^{-6}.$$

Given the linear polynomial (5.12) we can compute the first integral in (5.9) exactly. The time integrals in (5.9) are approximated by the midpoint rule and the flux integrals by the trapezium rule to give the staggered update

$$(5.17) \quad \begin{aligned} \bar{W}_{i+\frac{1}{2},j+\frac{1}{2}}^{n+1} &= \frac{1}{4} (\bar{W}_{i,j}^n + \bar{W}_{i+1,j}^n + \bar{W}_{i+1,j+1}^n + \bar{W}_{i,j+1}^n) \\ &+ \frac{1}{16} (W'_{i,j} - W'_{i+1,j} - W'_{i+1,j+1} + W'_{i,j+1}) \\ &+ \frac{1}{16} (W^\wedge_{i,j} + W^\wedge_{i+1,j} - W^\wedge_{i+1,j+1} - W^\wedge_{i,j+1}) \\ &- \frac{\lambda_1}{2} \left(F_1 \left(W_{i+1,j}^{n+\frac{1}{2}} \right) - F_1 \left(W_{i,j}^{n+\frac{1}{2}} \right) + F_1 \left(W_{i+1,j+1}^{n+\frac{1}{2}} \right) - F_1 \left(W_{i,j+1}^{n+\frac{1}{2}} \right) \right) \\ &- \frac{\lambda_2}{2} \left(F_2 \left(W_{i,j+1}^{n+\frac{1}{2}} \right) - F_2 \left(W_{i,j}^{n+\frac{1}{2}} \right) + F_2 \left(W_{i+1,j+1}^{n+\frac{1}{2}} \right) - F_2 \left(W_{i+1,j}^{n+\frac{1}{2}} \right) \right). \end{aligned}$$

Note that in (5.17) the fluxes are to be evaluated at the midpoint values $W_{i,j}^{n+\frac{1}{2}}$. Since these midvalues are secured at the centers of their cells $C_{i,j}$, bounded away from the jump discontinuities along the edges, we may use a Taylor expansion and the differential form of the conservation law (5.1) to obtain

$$(5.18) \quad W_{i,j}^{n+\frac{1}{2}} = \bar{W}_{i,j}^n - \frac{\lambda_1}{2} F_1(W_{i,j}^n)' - \frac{\lambda_2}{2} F_2(W_{i,j}^n)^\wedge,$$

where the discrete derivatives of the flux functions F_1 and F_2 are calculated in the same way as (5.13); see [20] for more details.

It is to be noted that a numerical solution of 3-D KCL (2.9)–(2.10) has to be augmented by the condition (2.11) at any time; i.e., an additional constraint has to be imposed on the solution in each time step. Fortunately, this constraint is inherent to the equations; i.e., once fulfilled at the initial data, it is fulfilled for all times. Thus, this constraint does not change the character of the equations, as in the case of incompressible Euler equations. The constraint (2.11) is analogous to the solenoidal condition in the equations of ideal magnetohydrodynamics (MHD). It is well known from the MHD literature that numerical schemes which violate the divergence-free constraint produce spurious solutions. In what follows, we show that the staggered central scheme (5.9) preserves condition (2.11).

THEOREM 5.1. *The staggered central scheme (5.9) fulfills the condition (2.11).*

Proof. In both the staggered LxF scheme and NxT scheme, we approximate the flux integrals in (5.9) by the trapezium rule. The time integral is approximated in

the LxF scheme by the left rectangle rule ($\tau = t^n$), whereas in the NxT scheme it is by the midpoint rule ($\tau = t^{n+\frac{1}{2}}$). After these approximations, (5.9) gives

$$\begin{aligned}
 \bar{W}_{i+\frac{1}{2},j+\frac{1}{2}}^{n+1} &= \bar{W}_{i+\frac{1}{2},j+\frac{1}{2}}^n \\
 (5.19) \quad & - \frac{\Delta t}{2h} (F_1(W_{i+1,j+1}^*) + F_1(W_{i+1,j}^*) - F_1(W_{i,j+1}^*) - F_1(W_{i,j}^*)) \\
 & - \frac{\Delta t}{2h} (F_2(W_{i+1,j+1}^*) + F_2(W_{i,j+1}^*) - F_1(W_{i+1,j}^*) - F_1(W_{i,j}^*)),
 \end{aligned}$$

where $W_{i,j}^*$ is a shortcut for $W(\xi_{1i}, \xi_{2j}, t^*)$ with $t^* = t^n$ or $t^{n+\frac{1}{2}}$. Let us introduce the finite difference operators

$$\begin{aligned}
 (5.20) \quad \delta_\xi \omega(\xi) &:= \omega\left(\xi + \frac{h}{2}\right) - \omega\left(\xi - \frac{h}{2}\right), \\
 \mu_\xi \omega(\xi) &:= \frac{1}{2} \left(\omega\left(\xi + \frac{h}{2}\right) + \omega\left(\xi - \frac{h}{2}\right) \right).
 \end{aligned}$$

Note that (5.19) can then be recast in the compact form

$$(5.21) \quad \bar{W}_{i+\frac{1}{2},j+\frac{1}{2}}^{n+1} = \bar{W}_{i+\frac{1}{2},j+\frac{1}{2}}^n - \frac{\Delta t}{h} \delta_{\xi_1} \mu_{\xi_2} F_1(W_{i,j}^*) - \frac{\Delta t}{h} \delta_{\xi_2} \mu_{\xi_1} F_2(W_{i,j}^*).$$

The use of (5.21) in the 3-D KCL system (5.1) results in

$$\begin{aligned}
 (5.22) \quad (g_1 \mathbf{u})_{i+\frac{1}{2},j+\frac{1}{2}}^{n+1} &= (g_1 \mathbf{u})_{i+\frac{1}{2},j+\frac{1}{2}}^n + \frac{\Delta t}{h} \delta_{\xi_1} \mu_{\xi_2} (m\mathbf{n})_{i+\frac{1}{2},j+\frac{1}{2}}^*, \\
 (g_2 \mathbf{v})_{i+\frac{1}{2},j+\frac{1}{2}}^{n+1} &= (g_2 \mathbf{v})_{i+\frac{1}{2},j+\frac{1}{2}}^n + \frac{\Delta t}{h} \delta_{\xi_2} \mu_{\xi_1} (m\mathbf{n})_{i+\frac{1}{2},j+\frac{1}{2}}^*.
 \end{aligned}$$

We approximate $(g_1 \mathbf{u})_{\xi_1} - (g_2 \mathbf{v})_{\xi_2}$ in a vertex centered manner,

$$(5.23) \quad (g_1 \mathbf{u})_{\xi_1} - (g_2 \mathbf{v})_{\xi_2}|_{i+\frac{1}{2},j+\frac{1}{2}} := \mu_{\xi_2} \delta_{\xi_1} (g_2 \mathbf{v})_{i+\frac{1}{2},j+\frac{1}{2}} - \mu_{\xi_1} \delta_{\xi_2} (g_1 \mathbf{u})_{i+\frac{1}{2},j+\frac{1}{2}}.$$

Therefore,

$$\begin{aligned}
 (g_1 \mathbf{u})_{\xi_1} - (g_2 \mathbf{v})_{\xi_2}|_{i+\frac{1}{2},j+\frac{1}{2}}^{n+1} &= \mu_{\xi_2} \delta_{\xi_1} (g_2 \mathbf{v})_{i+\frac{1}{2},j+\frac{1}{2}}^{n+1} - \mu_{\xi_1} \delta_{\xi_2} (g_1 \mathbf{u})_{i+\frac{1}{2},j+\frac{1}{2}}^{n+1} \\
 &= \mu_{\xi_2} \delta_{\xi_1} (g_2 \mathbf{v})_{i+\frac{1}{2},j+\frac{1}{2}}^n - \mu_{\xi_1} \delta_{\xi_2} (g_1 \mathbf{u})_{i+\frac{1}{2},j+\frac{1}{2}}^n \quad \text{using (5.22)} \\
 &= (g_1 \mathbf{u})_{\xi_1} - (g_2 \mathbf{v})_{\xi_2}|_{i+\frac{1}{2},j+\frac{1}{2}}^n.
 \end{aligned}$$

Thus, if the compatibility condition (2.11) is satisfied at $t = t^n$, then the staggered central scheme (5.9) preserves it at $t = t^{n+1}$. \square

Remark 5.2. It is well known from the literature that the solution of a Cauchy problem for a degenerate hyperbolic system (with incomplete eigenspace of dimension one less than the multiplicity of a multiple eigenvalue) contains a mode having linear growth in time. This component, the so-called Jordan mode, is in the direction of the corresponding generalized eigenvector. However, the results of our numerical experiments do not exhibit such a component. In order to understand the reason for the disappearance of the Jordan mode, we have studied the solution of the linearized version of the 3-D WNLRT system (5.1). The exact solution of the linearized system shows that the Jordan mode disappears when the constraint (2.11) is satisfied. Since the staggered central scheme (5.9) also preserves the constraint (2.11), the Jordan mode does not appear in the numerical results.

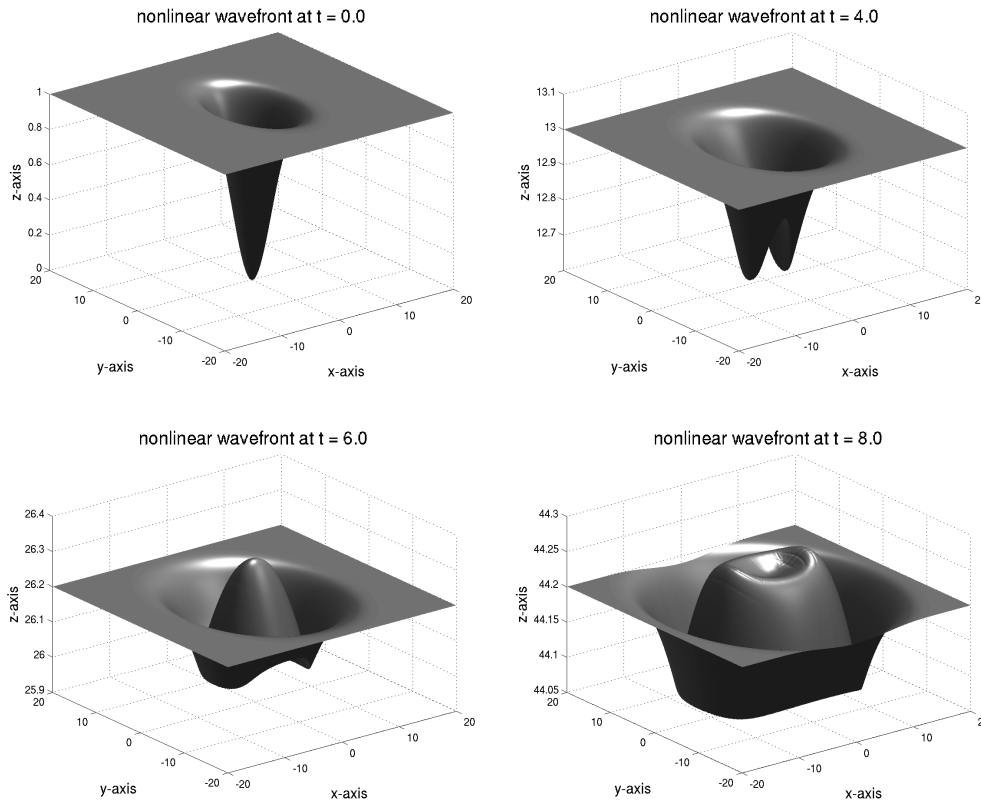


FIG. 6.1. The successive positions of the nonlinear wavefront Ω_t with an initial smooth non-symmetric dip which is not axisymmetric.

6. Numerical case studies. In order to demonstrate applicability of the 3-D KCL for modeling of time evolution of nonlinear wavefronts, we present in this section a few illustrating examples. Interesting phenomena, such as kink lines and kink curves, can be noticed in the physical (x_1, x_2, x_3) -space.

6.1. Propagation of a nonlinear wavefront which is not axisymmetric.

We choose initial wavefront Ω_0 in such a way that it is not axisymmetric. The front Ω_0 has a single smooth dip. The initial data reads

$$(6.1) \quad \Omega_0: x_3 = \kappa \left(1 - e^{-\left(\frac{x_1^2}{a^2} + \frac{x_2^2}{b^2}\right)} \right),$$

where the parameter values are set to be $\kappa = 3, a = 4, b = 8$.

The computational domain $[-20, 20] \times [-20, 20]$ is divided into 401×401 mesh points. The simulations are done for $t = 4.0, 6.0, 8.0$ with the NxT scheme with a CFL number 0.45.

In Figure 6.1, we plot the initial wavefront Ω_0 and the successive positions of the wavefront Ω_t at times $t = 4.0, 6.0, 8.0$. It can be seen that the wavefront has moved up in the x_3 -direction and the dip has spread over a larger area in the x_1 - and x_2 -directions. The lower part of the front moves up, leading to a change in shape of the initial front Ω_0 . Since the central portion becomes convex at $t = 6$ the rays

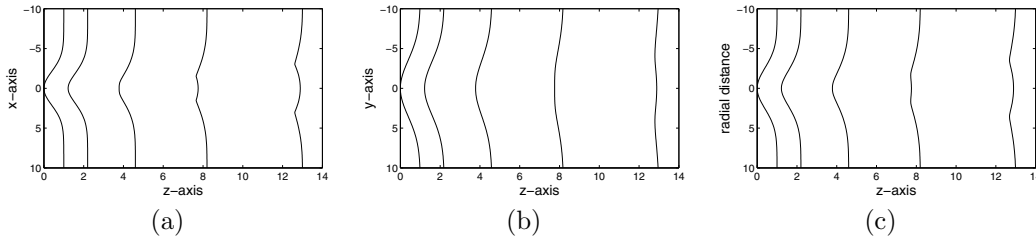


FIG. 6.2. The sections of the nonlinear wavefront in the (a) $y = 0$ -plane, (b) $x = 0$ -plane, and (c) $x = y$ -plane at times $t = 0.0, 1.0, 2.0, 3.0, 4.0$.

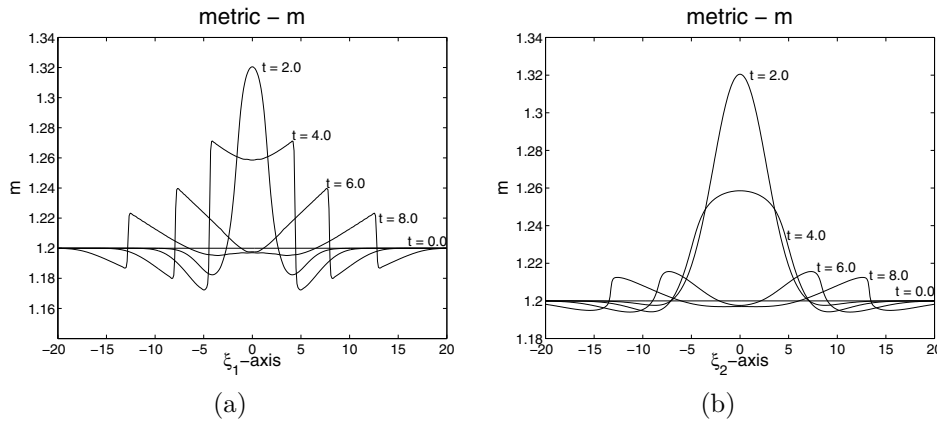


FIG. 6.3. The time evolution of the normal velocity m along the (a) ξ_1 -direction in section $\xi_2 = 0$, and (b) ξ_2 -direction in section $\xi_1 = 0$.

diverge from there, and as a result the front velocity decreases. It can be observed from the front at time $t = 8.0$ that the middle part of the upper portion goes down and becomes concave.

To explain the results of convergence of the rays, we also give in Figures 6.2(a), (b), and (c) the slices of the wavefront in $y = 0$ -section, $x = 0$ -section, and $x = y$ -section, respectively, from time $t = 0.0$ to $t = 4.0$. Due to the particular choice of the parameters a and b in the initial data (6.1), the section of the front Ω_0 in the $y = 0$ -plane has a smaller principal radius of curvature than that of the section in the $x = 0$ -plane. This results in a stronger convergence of the rays in the $y = 0$ -plane compared to the those in the $x = 0$ -plane, as is evident from Figures 6.2(a) and (b). The slice (c) along the diagonal plane $x = y$ shows an intermediate effect. In Figure 6.2(a), we clearly note a pair of kinks at time $t = 3.0$, which we can see in Figure 6.2(c) at time $t = 4.0$, but there are no kinks in Figure 6.2(b).

We give now the plots of the normal velocity m in the (ξ_1, ξ_2) -plane along the ξ_1 - and ξ_2 -directions in Figure 6.3. It is observed that m has two shocks in the ξ_1 -direction, which corresponds to the two kinks in the x -direction.

6.2. Comparison of 2-D and 3-D KCL results. Suppose in the initial data (6.1) we choose $a = b$; then the initial wavefront Ω_0 will be axisymmetric,

$$(6.2) \quad \Omega_0: x_3 = \kappa \left(1 - e^{-\frac{r^2}{a^2}} \right),$$

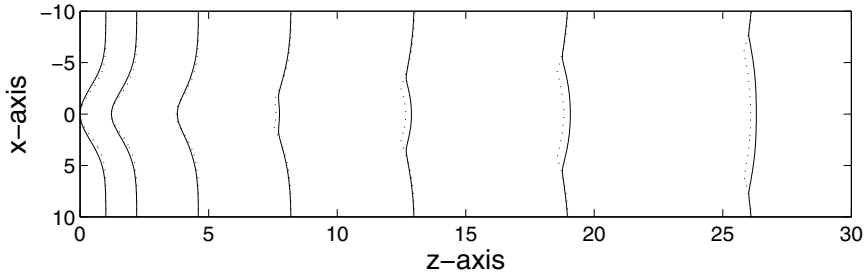


FIG. 6.4. Comparison of 3-D KCL and 2-D KCL: the solid lines represent the slices of 3-D wavefronts and the dotted lines are the 2-D wavefronts at times $t = 0.0$ to $t = 6.0$. The parameter $a = 4$.

where $r = \sqrt{x_1^2 + x_2^2}$ is the distance from the z -axis. The propagation of a 3-D nonlinear wavefront Ω_t with initial data (6.2) is axisymmetric and now reduces to an essentially 2-D problem with an additional source term due to axisymmetry, analogous to the axisymmetric Euler equations. We have also used the 2-D KCL without the additional axisymmetry term to study the time evolution of an essentially 2-D wavefront Ω_t . In order to illustrate the genuinely 3-D effects of geometrical convergence, we plot the corresponding results obtained from the 2-D KCL and the 3-D KCL in Figure 6.4. In this figure, the solid lines represent the successive nonlinear wavefronts obtained by the 3-D KCL, whereas the dotted lines represent the corresponding 2-D wavefronts obtained using 2-D KCL simulations. It can be observed that both results agree qualitatively. But the 2-D and 3-D wavefronts coincide only for small times; the 3-D wavefronts move faster than the 2-D ones. This shows the effect of truly 3-D geometrical convergence.

6.3. Propagation of an axisymmetric nonlinear wavefront having an initial smooth elevation. In this test case we choose the initial wavefront Ω_0 in the shape of an elevated Gaussian pulse,

$$(6.3) \quad \Omega_0 : x_3 = \kappa \left(1 + e^{-\left(\frac{x_1^2}{a^2} + \frac{x_2^2}{b^2}\right)} \right),$$

where the parameters are chosen to be $\kappa = 3$, $a = b = 4$.

The computational domain $[-20, 20] \times [-20, 20]$ is divided into 401×401 equal mesh points. The numerical simulations are done using the second order NxT scheme with a CFL number 0.45.

Figure 6.5 shows the successive nonlinear wavefronts at times $t = 4.0, 8.0, 16.0$. It can be observed that the whole wavefront has moved up and its height has decreased. The dent spreads over a larger area. The two kink circles are clearly visible at time $t = 8.0$. The central part of the front being convex, the rays diverge, whereas from the concave lower part they converge. As a result of this, the front velocity m decreases at the top in the central part and increases at the bottom. Due to this phenomenon, the outer portion moves up faster and tends to overtake the bulged portion, as evident from the front at $t = 16.0$.

We have also plotted the sections of the wavefront in the $y = 0$ -plane and the distribution of m with ξ_1 for $\xi_2 = 0$ in Figure 6.6. From Figure 6.6(b) it can be noted that there are four shocks in m at $t = 8.0$ and $t = 16$ which are mapped onto the four kinks on the front in Figure 6.6(a).

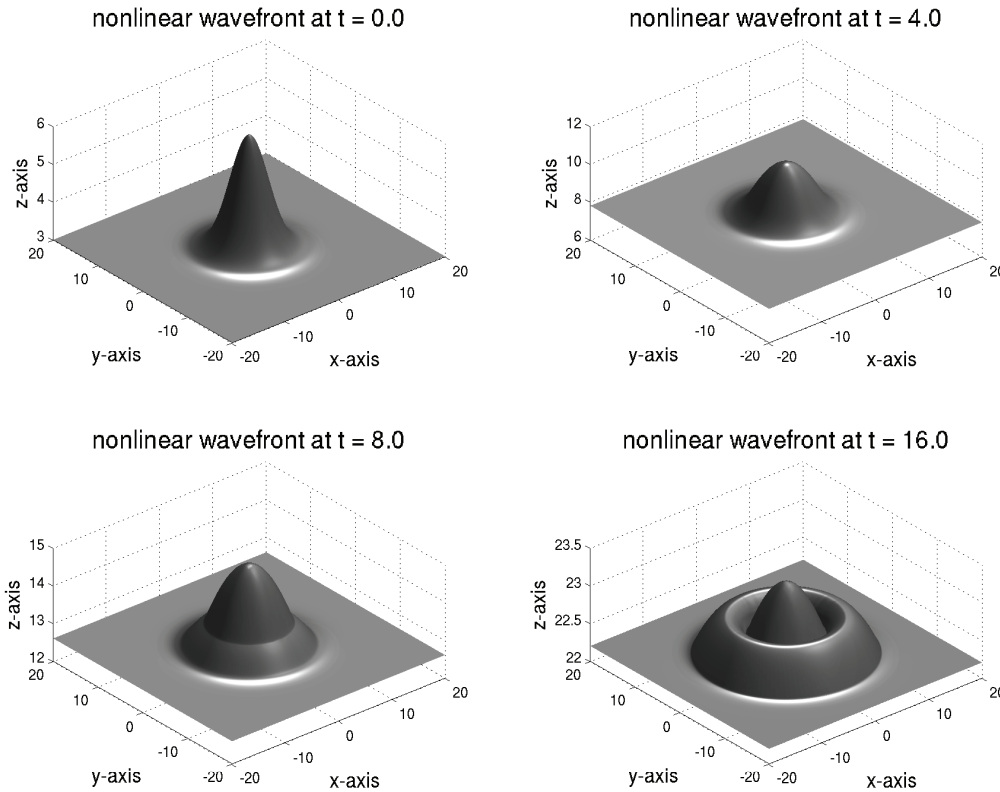


FIG. 6.5. The evolution of a nonlinear wavefront Ω_t starting from an elevated Gaussian pulse.

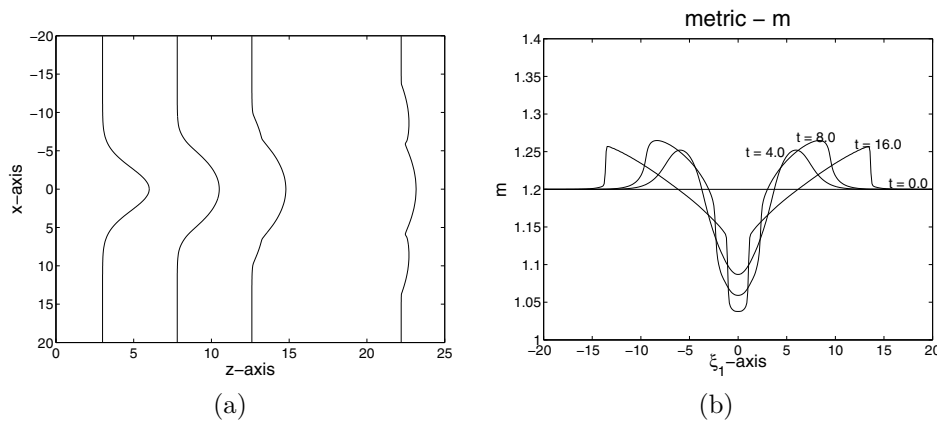


FIG. 6.6. (a) The slices of the wavefronts along $y = 0$. (b) The distribution of m with respect to ξ_1 along $\xi_2 = 0$.

6.4. Corrugational stability of a nonlinear wavefront. By “corrugational stability” we mean the stability of a plane front. The corrugational stability of plane shock fronts was first discussed by Gardner and Kruskal [16] in the context of MHD. Whitham [35] used his theory of shock dynamics to study this problem. Anile and

Russo [1] obtained an exact stability criterion for plane relativistic shock waves. The WNLRT is a very powerful method to study the corrugational stability of a nonlinear wavefront. The extensive numerical computations by Prasad and Sangeeta [29] with 2-D WNLRT show that a planar nonlinear wavefront in 2-D is stable; see also [24] for a discussion of corrugation stability of a 2-D shock front.

Here we intend to study the corrugation stability of a 3-D nonlinear wavefront using WNLRT. We choose the initial front to be of a periodic shape,

$$(6.4) \quad \Omega_0: x_3 = \kappa \left(2 - \cos\left(\frac{\pi x_1}{a}\right) - \cos\left(\frac{\pi x_2}{b}\right) \right),$$

with the constants $\kappa = 0.4$, $a = b = 2$. The initial velocity has a constant value $m_0 = 1.2$. The computational domain $[-4, 4] \times [-4, 4]$ is divided into 401×401 mesh points. The simulations are with the staggered LxF scheme for $t = 4.0, 8.0, 16.0, 20.0$ with a CFL number 0.25. In Figure 6.7 we give surface plots of the initial wavefront Ω_0 and the wavefronts Ω_t at times $t = 4.0, 8.0, 16.0, 20.0$. The front Ω_t moves up in the x_3 -direction and has developed several kink lines. Four horizontal kinks appear in each period of the initial front Ω_0 . During its time evolution, the elevations and depressions on the front decrease, which shows that the wavefront tends to become planar, leading to corrugational stability.

In Figure 6.7 the wavefronts at times $t \geq 8$ show a very complex pattern of kink lines; some are horizontal and very clear in the figure. To get a better feeling of this phenomenon, in Figure 6.8 we plot a zoomed portion in one period of the wavefront.

6.5. The effect of curvature on convergence of rays. In this test problem the initial wavefront Ω_0 is taken to be a part of an axisymmetric paraboloid extended by the tangent conoid given in the following way:

$$(6.5) \quad x_3 = \begin{cases} \kappa (x_1^2 + x_2^2) & \text{if } 0 \leq x_3 \leq 1, \\ 2\sqrt{\kappa}(x_1^2 + x_2^2)^{1/2} - 1 & \text{otherwise.} \end{cases}$$

In [24, 29] an analogous 2-D test problem was considered. However, as in the previous test problems we observe a stronger convergence of rays in the 3-D case. We study this problem for a value of the parameter $\kappa = 1/8$. In Figure 6.9 the computational result obtained by the second order scheme for $t = 4.0$ is presented. We have used a grid with 201×201 cells and have set the CFL number to 0.45. The slopes in the linear recovery were limited using the CWENO limiter. Exactly the same results were obtained by the first order staggered LxF scheme. From Figure 6.9 it can be observed that the wavefront moves up and its bottom tends to become more flat. A circular kink line appears which separates the upper curved surface from the plane base. In order to get a better visualization of this phenomenon, in Figure 6.10 we give the slices of the wavefronts along the $y = 0$ -plane together with the variation of m with respect to ξ_1 along $\xi_2 = 0$. It is to be noted that the results are in good qualitative agreement with the results of [29].

We have also studied this test problem for some larger value of κ , say $\kappa = 3/4$. In this case the curvature of the initial wavefront at the bottom becomes large so that the convergence of the rays is quite strong, and the shape of the wavefront ultimately develops a fold at the bottom, as is the case of linear caustics. Then in the numerical solution, the value of $m - 1$ becomes too large after some time and the scheme becomes unstable and computation fails. The result is certainly a valid solution of the 3-D KCL till the formation of the fold, but is not a physically realistic solution for the wave

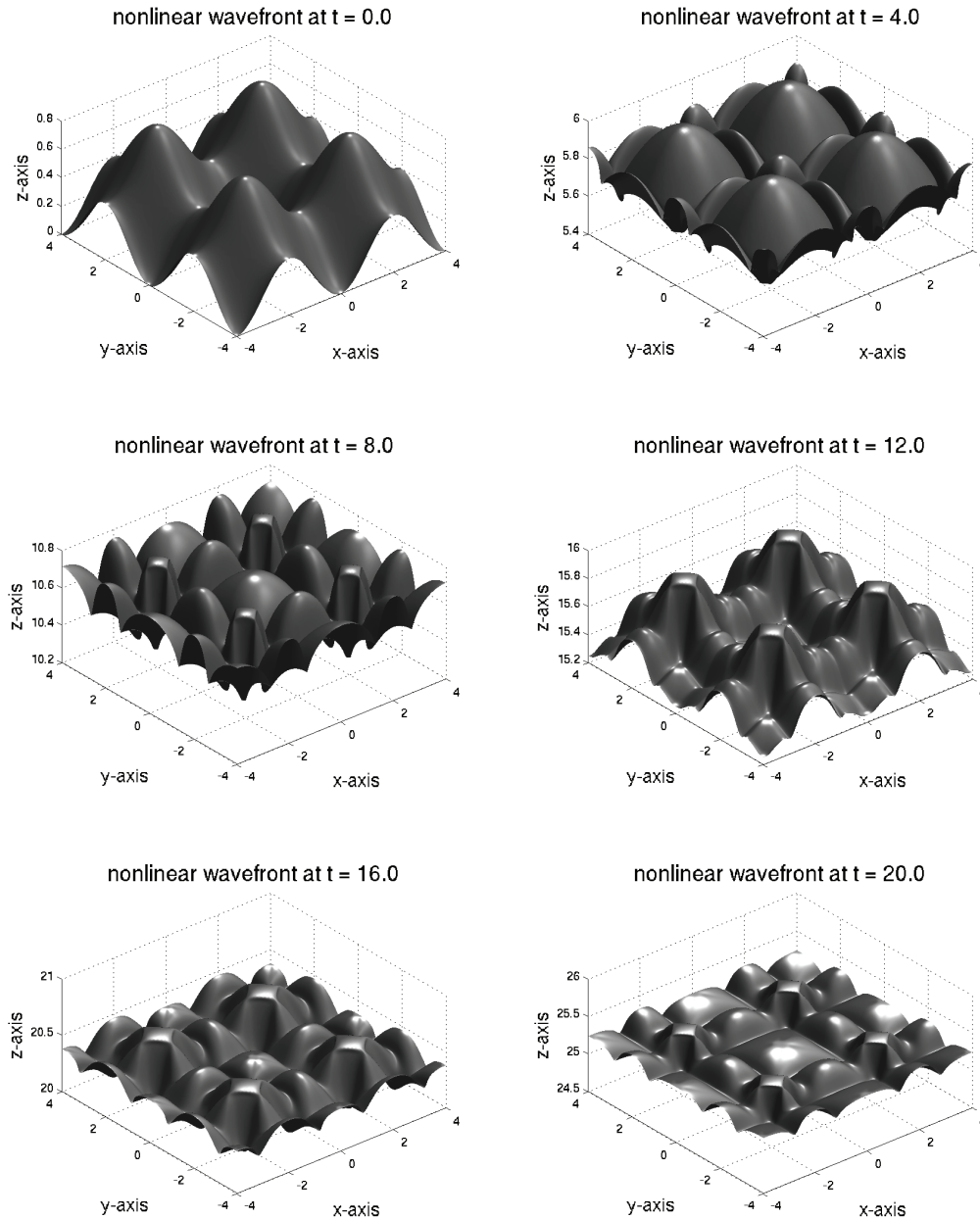


FIG. 6.7. Nonlinear wavefront Ω_t starting initially in a periodic shape with $m_0 = 1.2$. The front develops a complex pattern of kinks and ultimately becomes planar.

propagation since the values of $m - 1$ are too large for the WNLRT to be valid. We have numerically studied this problem extensively in two space dimensions by 2-D KCL (which is not degenerate but strictly hyperbolic). The solution shows the same behavior—a fold appears when initial curvature of the wavefront is large. The appearance of a fold and breakdown of the solution are not due to the appearance of the Jordan mode (as the constraint is initially satisfied), but the appearance of a fold

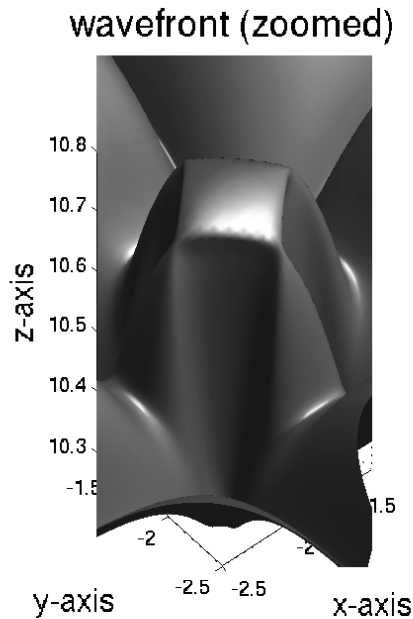


FIG. 6.8. A zoomed portion of the periodic nonlinear wavefront Ω_t in one period at time $t = 8.0$. The wavefront shows four horizontal kink lines forming the boundary of a square and two slanted ones in the background behind it.

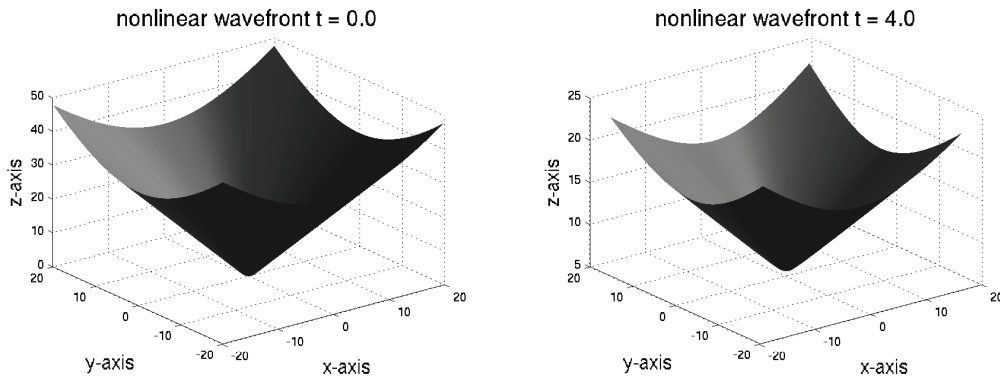


FIG. 6.9. Nonlinear wavefront Ω_t initially in a parabolic shape. On the left: initial wavefront at $t = 0.0$. On the right: the wavefront at $t = 4.0$. The value of the parameter $\kappa = \frac{1}{8}$.

is an inherent property of the waves. A detailed investigation of this aspect of the 2-D KCL and 3-D KCL is under way, and we shall report it later. The appearance of a fold in the numerical solution is important, as in the physical phenomena a fold does appear; see the experimental results in [31].

Acknowledgments. The authors sincerely thank the unknown referees for their extremely valuable comments and Professor Tommaso Ruggeri for personal discussion, which lead to a considerable improvement of the paper.

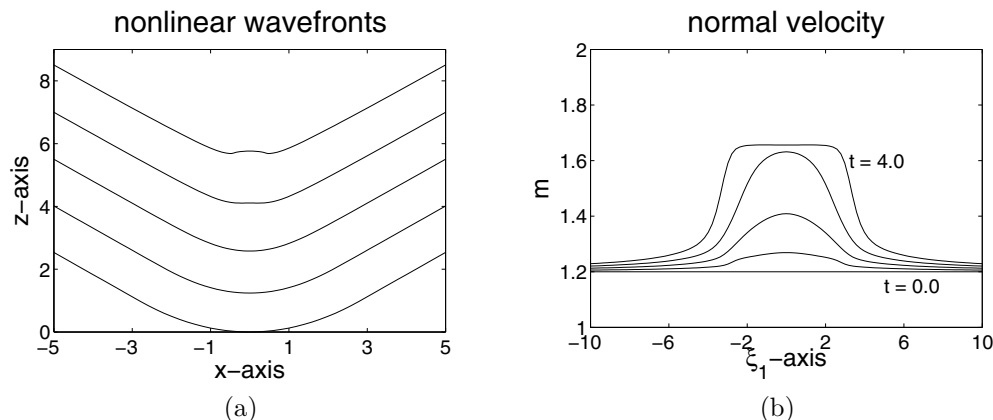


FIG. 6.10. (a) Slices of the nonlinear wavefronts along $y = 0$. (b) The distribution of m with respect to ξ_1 for the problem with initial data (6.5) with $\kappa = \frac{1}{8}$.

REFERENCES

- [1] A. M. ANILE AND G. RUSSO, *Corrugation stability for plane relativistic shock waves*, Phys. Fluids, 29 (1986), pp. 2847–2852.
- [2] P. ARMINJON, M. C. VIALON, AND A. MADRANE, *A finite volume extension of the Lax-Friedrichs and Nessyahu-Tadmor schemes for conservation laws on unstructured grids*, Int. J. Comput. Fluid Dyn., 9 (1997), pp. 1–22.
- [3] K. R. ARUN AND P. PRASAD, *3-D kinematical conservation laws (KCL): Evolution of a surface in \mathbb{R}^3 —in particular propagation of a nonlinear wavefront*, Wave Motion, 46 (2009), pp. 293–311.
- [4] K. R. ARUN AND P. PRASAD, *Eigenvalues of kinematical conservation laws (KCL) based 3-D weakly nonlinear ray theory (WNLRT)*, Appl. Math. Comput. to appear.
- [5] S. BASKAR AND P. PRASAD, *Kinematical conservation laws applied to study geometrical shapes of a solitary wave*, in Wind over Waves II: Forecasting and Fundamentals, S. Sajjadi and J. Hunt, eds., Horwood, Chichester, UK, 2003, pp. 189–200.
- [6] S. BASKAR AND P. PRASAD, *Riemann problem for kinematical conservation laws and geometrical features of nonlinear wavefronts*, IMA J. Appl. Math., 69 (2004), pp. 391–420.
- [7] S. BASKAR AND P. PRASAD, *Propagation of curved shock fronts using shock ray theory and comparison with other theories*, J. Fluid Mech., 523 (2005), pp. 171–198.
- [8] S. BASKAR AND P. PRASAD, *Formulation of the problem of sonic boom by a maneuvering aerofoil as a one parameter family of Cauchy problems*, Proc. Indian Acad. Sci. (Math. Sci.), 116 (2006), pp. 97–119.
- [9] F. BOUCHUT, *On zero pressure gas dynamics*, in Advances in Kinetic Theory and Computing, Ser. Adv. Math. Appl. Sci. 22, World Scientific, River Edge, NJ, 1994, pp. 171–190.
- [10] F. BOUCHUT, S. JIN, AND X. LI, *Numerical approximations of pressureless and isothermal gas dynamics*, SIAM J. Numer. Anal., 41 (2003), pp. 135–158.
- [11] Y. BRENIER AND E. GRENIER, *Sticky particles and scalar conservation laws*, SIAM J. Numer. Anal., 35 (1998), pp. 2317–2328.
- [12] G. Q. CHEN AND P. T. KAN, *Hyperbolic conservation laws with umbilic degeneracy (I)*, Arch. Ration. Mech. Anal., 130 (1995), pp. 231–276.
- [13] R. COURANT AND F. JOHN, *Introduction to Calculus and Analysis*, Vol. II, John Wiley & Sons, New York, 1974.
- [14] V. G. DANILOV AND D. MITROVIC, *Delta shock wave formation in the case of triangular hyperbolic system of conservation laws*, J. Differential Equations, 245 (2008), pp. 3704–3734.
- [15] B. ENQUIST AND O. RUNBORG, *Multi-phase computations in geometrical optics*, J. Comput. Appl. Math., 74 (1996), pp. 175–192.
- [16] C. S. GARDNER AND M. D. KRUSKAL, *Stability of plane magnetohydrodynamic shocks*, Phys. Fluids, 7 (1964), pp. 700–706.
- [17] M. GILES, P. PRASAD, AND R. RAVINDRAN, *Conservation Form of Equations of Three Dimensional Front Propagation*, Technical report, Department of Mathematics, Indian Institute of Science, Bangalore, 1995.

- [18] F. HUANG, *Existence and uniqueness of discontinuous solutions for a class of non-strictly hyperbolic systems*, in *Advances in Nonlinear Partial Differential Equations and Related Areas* (Beijing, 1997), World Scientific, River Edge, NJ, 1998, pp. 187–208.
- [19] G. S. JIANG AND C. W. SHU, *Efficient implementation of weighted ENO schemes*, *J. Comput. Phys.*, 126 (1996), pp. 202–228.
- [20] G.-S. JIANG AND E. TADMOR, *Nonoscillatory central schemes for multidimensional hyperbolic conservation laws*, *SIAM J. Sci. Comput.*, 19 (1998), pp. 1892–1917.
- [21] G.-S. JIANG, D. LEVY, C.-T. LIN, S. OSHER, AND E. TADMOR, *High-resolution nonoscillatory central schemes with nonstaggered grids for hyperbolic conservation laws*, *SIAM J. Numer. Anal.*, 35 (1998), pp. 2147–2168.
- [22] P. LAX, *Weak solutions of nonlinear hyperbolic equations and their numerical computation*, *Comm. Pure Appl. Math.*, 7 (1954), pp. 159–193.
- [23] R. J. LEVEQUE, *The dynamics of pressureless dust clouds and delta waves*, *J. Hyperbolic Differ. Equ.*, 1 (2004), pp. 315–327.
- [24] A. MONICA AND P. PRASAD, *Propagation of a curved weak shock*, *J. Fluid Mech.*, 434 (2001), pp. 119–151.
- [25] K. W. MORTON, P. PRASAD, AND R. RAVINDRAN, *Conservation Form of Nonlinear Ray Equations*, Technical report, Department of Mathematics, Indian Institute of Science, Bangalore, 1992.
- [26] H. NESSYAHU AND E. TADMOR, *Non-oscillatory central differencing for hyperbolic conservation laws*, *J. Comput. Phys.*, 87 (1990), pp. 408–463.
- [27] P. PRASAD, *Nonlinear Hyperbolic Waves in Multi-dimensions*, Chapman Hall/CRC Monogr. Surv. Pure Appl. Math. 121, Chapman and Hall/CRC, Boca Raton, FL, 2001.
- [28] P. PRASAD, *Ray theories for hyperbolic waves, kinematical conservation laws (KCL) and applications*, *Indian J. Pure Appl. Math.*, 38 (2007), pp. 467–490.
- [29] P. PRASAD AND K. SANGEETA, *Numerical simulation of converging nonlinear wavefronts*, *J. Fluid Mech.*, 385 (1999), pp. 1–20.
- [30] V. M. SHELKOVICH, *Multidimensional Delta-Shocks and the Transportation and Concentration Processes*, preprint, 2007; available on <http://www.math.ntnu.no/conservation/2007/031.html>.
- [31] B. STURTEVANT AND V. A. KULKARNY, *The focusing of weak shock waves*, *J. Fluid Mech.*, 73 (1976), pp. 651–671.
- [32] O. RUNBORG, *Some new results in multiphase geometrical optics*, *M2AN Math. Model. Numer. Anal.*, 34 (2000), pp. 1203–1231.
- [33] D. TAN, T. ZHANG, AND Y. ZHENG, *Delta-shock waves as limits of vanishing viscosity for hyperbolic systems of conservation laws*, *J. Differential Equations*, 112 (1994), pp. 1–32.
- [34] G. B. WHITHAM, *A new approach to problems of shock dynamics. I. Two dimensional problems*, *J. Fluid Mech.*, 2 (1957), pp. 145–171.
- [35] G. B. WHITHAM, *Linear and Nonlinear Waves*, John Wiley & Sons, New York, 1974.